

A search for the submillimetre counterparts to Lyman break galaxies

Scott C. Chapman,^{1,2} Douglas Scott,¹ Charles C. Steidel,³ Colin Borys,¹
Mark Halpern,¹ Simon L. Morris,⁴ Kurt L. Adelberger,³ Mark Dickinson,⁵
Mauro Giavalisco⁵ and Max Pettini⁶

¹*Department of Physics & Astronomy, University of British Columbia, Vancouver, B.C. V6T 1Z1, Canada*

²*Present address: Observatories of the Carnegie Institution of Washington, Pasadena, CA 91101, U.S.A.*

³*Palomar Observatory, Caltech 105-24, Pasadena, CA 91125, U.S.A.*

⁴*National Research Council of Canada, Herzberg Institute of Astrophysics, Victoria, B.C. V8X 4M6, Canada*

⁵*Space Telescope Science Institute, 3700 San Martin Drive, Baltimore, MD 21218, U.S.A.*

⁶*Institute of Astronomy, Madingley Road, Cambridge CB3 0HA, U.K.*

Submitted to Mon. Not. R. astr. Soc.

ABSTRACT

We have carried out targetted sub-mm observations as part of a programme to explore the connection between the rest-frame UV and far-IR properties of star-forming galaxies at high redshift, which is currently poorly understood. On the one hand the Lyman break technique is very effective at selecting $z \sim 3$ galaxies. On the other hand ‘blank field’ imaging in the sub-mm seems to turn up sources routinely, amongst which some are star forming galaxies at similar redshifts. Already much work has been done searching for optical identifications of objects detected using the SCUBA instrument. Here we have taken the opposite approach, performing sub-mm photometry for a sample of Lyman break galaxies whose UV properties imply high star formation rates.

The total signal from our Lyman break sample is undetected in the sub-mm, at an rms level of ~ 0.5 mJy, which implies that the population of Lyman break galaxies does not constitute a large part of the recently detected blank-field sub-mm sources. However, our one detection suggests that with reasonable SCUBA integrations we might expect to detect those few LBGs that are far-IR brightest.

Key words: galaxies: starburst – galaxies: active – galaxies: formation – cosmology: observations – infrared: galaxies

1 INTRODUCTION

Using a variety of techniques in different wavebands, the detailed study of young galaxies is being pushed to higher redshifts. The method of selecting high redshift galaxies using multi-colour broadband observations of the rest-frame UV stellar continuum has been successfully applied to ground-based surveys, and also to the Hubble Deep Field (HDF). In particular, the absence of emission in the U -band at $z \sim 3$ due to the presence of the Lyman break feature has been very effective (Steidel & Hamilton 1993; Steidel, Pettini & Hamilton 1995; Steidel et al. 1998), and is usually referred to as the Lyman break technique (e.g. Steidel et al. 1996a). A full characterization of the properties of the population of galaxies chosen in this way, called Lyman break galaxies (LBGs), will likely provide answers to some key questions of

galaxy formation and evolution, particularly those dealing with the murky role of dust at high redshift.

The colours of Lyman break galaxies are observed to be redder than expected for dust-free star-forming objects. The spectral slope of the ultraviolet continuum and the strength of the $H\beta$ emission line suggest that some interstellar dust is already present in these young galaxies, and that it attenuates their UV luminosities by a factor of ~ 4.5 , although factors of as much as 100 are implied for some LBGs (Steidel et al. 1998). In the most extreme objects this implies star formation rates (SFRs) of several times $100 M_{\odot} \text{ yr}^{-1}$, reaching as high as $1000 M_{\odot} \text{ yr}^{-1}$ in some cases. The resulting revisions to the global star formation rate contributed by galaxies at redshifts $z > 2$ can be significant. However, the prescription for a ‘correct’ de-reddening is still unknown at present (see for example Meurer et al. 1997). This leads to an uncertainty in the estimates of dust obscuration in LBGs

derived from rest frame ultraviolet spectra (see e.g. Pettini et al. 1998; Calzetti et al. 1996).

The role dust plays in these young galaxies is not clear cut, since redder spectra can also occur from an aging population, or from an initial mass function (IMF) deficient in massive stars (see e.g. Bruzual & Charlot 1993). Recent studies of nearby star-forming galaxies (Tresse and Maddox 1998) have concluded that the extinction at a wavelength of 2000 Å is typically 1.2 mag. The situation at earlier epochs is unclear, but there is no need to assume that at higher redshifts an increasing fraction of the star formation activity takes place in highly obscured galaxies. The precise amounts of reddening required, and its interpretation, are therefore still open questions.

Observations using a sensitive new bolometric array, SCUBA on the JCMT (described in section 2), have discovered a population of submillimetre detected galaxies (Smail et al. 1997; Hughes et al. 1998; Barger et al. 1998; Eales et al. 1999; Holland et al. 1998; Blain et al. 1999b) which might push up the global SFR at $z \sim 3$ by a factor of perhaps five (see for example Smail et al. 1997). Identifying the optical counterparts to these galaxies, however, is a non-trivial matter for two main reasons: 1) the SCUBA beamsizes at 850 μm (the optimal wavelength for these studies) is ~ 15 arcsec, with pointing errors for the telescope of order 2 arcsec; 2) the large, negative K-corrections of dusty star-forming galaxies at these wavelengths (i.e. the increase in flux density as the objects are redshifted, because of the steep spectrum of cool dust emission) imply that sub-mm observations detect such objects at $z > 1$ in an almost distance-independent manner (Blain & Longair 1993). Thus several candidate optical galaxies are often present within the positional uncertainty of the sub-mm detection, and there is a very strong possibility that the actual counterpart is at much higher redshift and undetectable with current optical imaging. Because of these difficulties, it is presently unknown whether these newly discovered sub-mm galaxies are drawn from a population similar to the LBGs, or whether the two methods select entirely different types of object at similar redshifts.

Attention has so far focussed on constraining SCUBA source counts and using follow-up observations in other wavebands to identify the sub-mm galaxies. Direct estimates of the source counts have recently come from several survey projects covering small regions on the sky to 3σ sensitivities ranging from 0.5 mJy to 8 mJy (Smail et al. 1997; Hughes et al. 1998; Barger et al. 1998; Holland et al. 1998; Eales et al. 1999; Blain et al. 1999b; Chapman et al. 1999b). In addition, statistical upper limits can be put on the source counts at even fainter limits through fluctuation analysis of ‘blank field’ data (Hughes et al. 1998; Borys, Chapman & Scott 1999). There is currently some debate about what fraction of detected sources lie at redshifts above $z \sim 2$, and what fraction may be at more modest distances, $z < 1$ (see Hughes et al. 1998; Smail et al. 1998; Lilly et al. 1999; Barger et al. 1999). It is fair to say that the numbers are still so small, and the optical identification procedure still sufficiently ambiguous, that this debate is currently unresolved. Furthermore, the issue of the importance of AGN-fuelled star formation, i.e. the fraction of SCUBA-bright sources which are active galaxies, is also still an open issue (see e.g. Ivison et al. 1999a; Almaini et al. 1999).

A statistical estimate of the number density of LBGs

whose UV spectra imply $\text{SFR} > 400 \text{ M}_{\odot} \text{ yr}^{-1}$, after correcting for extinction and including photometric errors (Adelberger & Steidel 2000), results in a comoving number density that is roughly comparable to the comoving number density of SCUBA sources with this SFR (2000 per square degree – e.g. Eales et al. 1999; Blain et al. 1999b). This raises the question of whether the populations are the same or at least related, and whether, if the uncertainties were better constrained in the LBG population, and if more near-IR data were available, it would be relatively easy to select star-forming galaxies detectable with SCUBA.

In order to address these issues, we have targetted a sample of LBGs, which have high UV-estimated SFRs, for photometry in the sub-mm. The full sample of more than 700 LBGs which have spectroscopic redshifts (Steidel et al. in preparation) has a range of extinction implied by far-UV models from zero to a factor of more than 100. We have chosen a small number of candidates from this group whose UV properties indicate that they are the most likely to be detectable with SCUBA.

The sub-mm observations provide an estimate of the global dust mass and SFR which is unaffected by the obscuration uncertainties inherent in the UV continuum, but on the other hand suffers from many model dependencies. Relating the SFRs obtained from the two wavelength regimes may help to elucidate the energetics of star formation in luminous star-forming galaxies. The bulk of this paper therefore focuses on comparison of SCUBA flux densities with UV-predicted 850 μm emission, or equivalently of the SFRs estimated from the rest-frame UV and far-IR wavebands.

2 OBSERVATIONS

A total of 16 LBGs were targetted in three different regions: the HDF flanking fields (Williams et al. 1996), the Westphal 14 hour field (also known as the ‘Groth Strip’, Groth et al. 1994), and several deep redshift survey fields at 22 hours (Steidel et al. in preparation). These are three of the regions for which extensive study of LBGs has already been carried out (see e.g. Steidel et al. 1996a).

Our initial choice of targets was based on the qualitative assumption that high UV-derived SFRs and bright magnitudes might imply large sub-mm fluxes. Hence the LBGs chosen for sub-mm observation had the largest SFRs inferred from the UV and optical data available at the time of observation, ranging from 360 to 860 $\text{M}_{\odot} \text{ yr}^{-1}$ (corresponding to 1.8–4.3 mJy at 850 μm). Subsequent careful analysis of the errors through Monte Carlo simulations (Adelberger & Steidel 2000) have shown that actually the brighter galaxies, with relatively small corrections to their UV SFRs, are more likely to have large sub-mm fluxes. In addition, optical spectral and imaging data, obtained subsequent to the sub-mm observations, also tended to lead to reductions in the initial estimates; in fact a few of the objects which had the most extreme reddening estimates turned out to be at much lower redshift. As a result, half of the original 16 LBGs targetted no longer have implied SFRs which would make them detectable with SCUBA. Nevertheless, it is still interesting to study carefully what the observed sample may be telling us.

Those objects with implied SFRs which place them at

a SCUBA flux density level of at least 0.5 mJy are included in Table 1. (In fact all have implied 850 μ m flux densities >1 mJy). The remaining objects are included in Table 2, and they can be regarded, in a sense, as a control sample. There are no redshift estimates for the objects in Table 2. Object names in the tables denote catalogue entries for these fields as discussed in Steidel et al. (in preparation).

2.1 Submillimetre observations

The observations were conducted with the Submillimetre Common-User Bolometer Array (SCUBA, Holland et al. 1999) on the James Clerk Maxwell Telescope. The data set was obtained over six nights from observing runs in May and June 1998. We operated the 91 element Short-wave array at 450 μ m and the 37 element Long-wave array at 850 μ m simultaneously in photometric mode, giving half-power beam widths of 7.5, and 14.7 arcsec respectively.

Conditions were generally reasonably good in May, with τ_{850} ranging from 0.31 to 0.40, and very good in June (τ_{850} =0.13–0.16). Observations were divided into scans lasting about 40 min for 100×18 s integrations. The usual 9-point jiggle pattern was employed to reduce the impact of pointing errors and thereby produce greater photometric accuracy by averaging the source signal over a slightly larger area than the beam. Whilst jiggling, the secondary was chopped by 45 arcsec in azimuth at the standard 7.8125 Hz. This mode allows deeper integration on the central pixel for a fixed observing time than in mapping mode. Pointing errors were below 2 arcsec, checked on nearby blazars every 80 min. The total exposure times and resulting rms sensitivities are listed in Tables 1 and 2.

The data were reduced using both the Starlink package SURF (Scuba User Reduction Facility, Jenness & Lightfoot 1998), and independently with our own routines (see Borys, Chapman & Scott 1999). Spikes were rejected from the double difference data, which were then corrected for atmospheric opacity and sky emission using the median of all the pixels except for the central pixel and any obviously bad pixels. We improved the effective sensitivity to source detection by incorporating the flux density in negative off-beam pixels of the LBG source, as described in the following subsection, and by removing possible sources in the field before estimating background flux levels; any bolometer that had a signal $> 2\sigma$ was removed from the sky estimation. Whether or not the negative beam bolometers were used in the sky subtraction made no discernible difference.

We have written routines which extend the capabilities of SURF by analysing the photometry of each bolometer independently, weighting each scan by its variance. This is crucial for data of the same object taken over several nights of observing. Our routines also allow us to characterise the noise spectrum and to check for residual gradients across the array. In practice, however, we found it was unnecessary to subtract gradients from this data set. Analysis of the entire array used in photometry mode is essential to extract meaningful numbers for faint signal levels, since we are approaching the noise levels for which source counts are beginning to make a sizable contribution to the background noise. Confusion limit is at ~ 1 mJy (Hughes et al. 1998). We discuss this further in Section 2.1.2.

We calibrated our data against Uranus and IRC 10216.

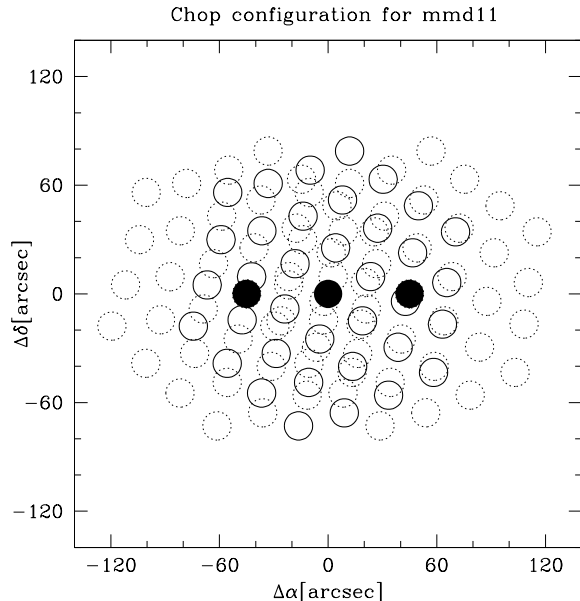


Figure 1. Chopping geometry. The SCUBA 850 μ m bolometer configuration on the sky is depicted. The solid filled circles give the position of the central bolometer in all three chop positions (the chop throw for these observations was 45 arcsec). The open circles with solid lines show the array in the central chop position, while the dashed circles give the off-beams. Clearly there will be some off-beams that chop on to the source, with an efficiency which varies as the array rotates relative to the sky.

The calibrations agree with each other, and with the gains found by other observers using SCUBA at around the same time, to within 10 per cent at 850 μ m, and to 20 per cent at 450 μ m, remaining stable night to night. Folding this calibration uncertainty in to our error budget has little effect at the low signal-to-noise ratio levels of these observations.

2.1.1 Folding in the off-beams

The signal from the off-beams that chop on to the source can be used to improve the estimate of the flux density from the source. For a source with flux density S , measured with an efficiency ϵ and measurement error σ , the probability that the measured value is x is given by:

$$P(x) \propto \exp \left[-\frac{1}{2} \left(\frac{x - \epsilon S}{\sigma} \right)^2 \right]. \quad (1)$$

By minimizing the joint probability of N measurements, the maximum likelihood estimator of the source flux density is

$$\bar{S} = \frac{\sum_i^N x'_i \sigma'^{-2}}{\sum_i^N \sigma'^{-2}}, \quad (2)$$

where $x' = x/\epsilon$ and $\sigma' = \sigma/\epsilon$.

As the sky rotates during an experiment, the effective efficiency, ϵ , for the off beams varies. Fig. 1 shows an illustration of this effect during our observations of W-MMD11. For our double-difference observations there are instantaneously $N = 3$ beams, with the central beam having an efficiency of unity and the two off beams having

Table 1. Sub-mm flux densities and other data for our targetted Lyman break galaxies (and those already covered by the Hughes et al. 1998 HDF integration), including only those objects with relatively high implied star formation rates. We give the galaxy designation, redshift, SCUBA integration time (total time chopping on and off source), observed 850 μm and 450 μm flux density and error, and the SCUBA-derived SFR upper limit in the first six columns. Columns 7 through 10 provide the associated optical parameters: R -band magnitude, the SFR derived from the raw UV flux and the UV-corrected SFR estimate, plus the 850 μm flux density predicted from the UV data. SFR estimates assume $\Omega_0 = 1$ and $h = 0.5$.

Galaxy	z	Sub-mm parameters					Restframe UV parameters			
		t (ksec)	$S_{850} \pm \sigma_{850}$ (mJy)	$S_{450} \pm \sigma_{450}$ (mJy)	$\text{SFR}_{850}^{\text{a}}$ ($\text{M}_{\odot} \text{ yr}^{-1}$)	R_{s} (mag)	$G - R_{\text{s}}$ (mag)	$\text{SFR}_{\text{UV}}^{\text{b}}$ ($\text{M}_{\odot} \text{ yr}^{-1}$)	$\text{SFR}_{\text{UV-corr}}^{\text{c}}$ ($\text{M}_{\odot} \text{ yr}^{-1}$)	$S_{850-\text{UV}}^{\text{d}}$ (mJy)
WESTPHAL FIELD										
W-DD20	3.083	9.0	-0.1 ± 0.9	-11 ± 10	< 190	23.1	1.2	51.2	193 ± 210	1.6 ± 1.8
W-MM27	2.789	9.0	-1.1 ± 1.0	$35 \pm 12^{\text{e}}$	< 120	24.1	1.0	20.5	175 ± 164	2.2 ± 1.5
W-MM8	2.829	5.4	0.7 ± 1.1	-8 ± 16	< 250	24.1	1.0	20.4	175 ± 164	1.5 ± 1.1
W-MMD109	2.715	9.0	1.4 ± 0.9	-7 ± 15	< 250	23.9	0.8	22.5	280 ± 173	1.8 ± 1.3
W-CC76	2.871	1.8	-1.7 ± 2.5	47 ± 54	< 390	23.3	0.8	37.9	201 ± 124	1.4 ± 0.8
W-CC1	2.984	5.4	0.5 ± 1.3	1 ± 20	< 310	23.8	1.0	25.5	152 ± 187	1.7 ± 1.4
W-MMD11	2.979	4.9	5.5 ± 1.4	22 ± 23	600 ± 150	24.1	1.0	21.0	173 ± 95	1.2 ± 0.6
W-MMD46	2.917	4.9	-0.6 ± 1.1	14 ± 16	< 190	23.8	0.9	26.7	138 ± 92	1.6 ± 1.0
MEAN ^f			0.51 ± 0.39	4.9 ± 5.3						1.46 ± 0.36
MEAN w/o W-MMD11			0.08 ± 0.41	3.9 ± 5.5						1.61 ± 0.44
HDF (Hughes et al. 1998)										
H-MM18	2.929	135 ^g	$< 1.2^{\text{h}}$	< 20	< 120	24.1	1.0	20.0	151 ± 96	1.1 ± 0.8
H-MM17	2.931	135	< 1.2	< 20	< 120	24.5	1.0	14.4	121 ± 86	0.7 ± 1.0

^a For the upper limits we quote the Bayesian 95 per cent value (i.e. excluding the unphysical negative flux region), assuming a 50 K dust temperature, as described in section 3.

^b Uncorrected, based on the UV flux.

^c Calzetti attenuation curve corrected, taking into account Monte Carlo simulations of the photometric errors. Simple rms errors are quoted, while in fact the distributions are skewed, and none of the predicted SFRs or flux densities could be negative. The order of the LBGs in this list reflects our original estimates for SFR.

^d Predicted from the UV colours, see section 3.

^e This possible detection at 450 μm is much more likely to be from a foreground object than the $z \sim 3$ galaxy.

^f Average flux from all targets, combined with inverse variance weighting.

^g Approximate 2σ upper limits estimated from Hughes et al. (1998).

^h The 51 hour integration on the HDF was done in ‘jiggle map’ mode to fully sample the field; it is roughly equivalent to a 10 hour ‘photometry’ integration.

Table 2. Sub-mm flux densities and other data from Lyman break galaxies originally on our target list, but which subsequently turned out to have significantly lower or uncertain estimates for star formation rate than those in Table 1. This can be considered as a control list, and we present the data for completeness. The objects in the various 22 hour fields were originally in our sample because they had extreme reddening estimates, but subsequently have turned out not to be LBGs, and probably lie at lower redshifts. They are not likely to be sub-mm emitters. Columns are as in Table 1.

Galaxy	z	Sub-mm parameters					Restframe UV parameters			
		t (ksec)	$S_{850} \pm \sigma_{850}$ (mJy)	$S_{450} \pm \sigma_{450}$ (mJy)	$\text{SFR}_{850}^{\text{a}}$ ($\text{M}_{\odot} \text{ yr}^{-1}$)	R_{s} (mag)	$G - R_{\text{s}}$ (mag)	$\text{SFR}_{\text{UV}}^{\text{b}}$ ($\text{M}_{\odot} \text{ yr}^{-1}$)	$\text{SFR}_{\text{UV-corr}}^{\text{c}}$ ($\text{M}_{\odot} \text{ yr}^{-1}$)	$S_{850-\text{UV}}^{\text{d}}$ (mJy)
HDF FLANKING FIELDS										
H-C38	3.114	3.6	0.6 ± 1.9	-144 ± 81	< 490	25.0	0.7	5.0	31.0 ± 28.0	0.14 ± 0.12
H-C10	2.985	3.6	-1.7 ± 1.8	129 ± 67	< 280	24.8	0.8	6.1	44.0 ± 20.1	0.10 ± 0.11
H-D2	2.982	1.8	-5.0 ± 3.1	-162 ± 107	< 400	25.2	0.7	0.4	2.1 ± 1.0	0.01 ± 0.04
22 HOUR FIELDS										
22A-MD6	—	7.2	0.1 ± 1.1	-6 ± 16	—	24.1	0.9	—	—	—
CDFA-M17	—	5.4	-0.7 ± 1.1	10 ± 14	—	24.6	1.0	—	—	—
22A-MD55	—	5.4	-1.9 ± 1.1	21 ± 12	—	24.4	0.9	—	—	—
DSF22A-D2	—	3.6	1.0 ± 1.2	-1 ± 13	—	23.8	0.7	—	—	—
22B-MD36	—	3.6	0.0 ± 1.2	-2 ± 12	—	23.2	0.8	—	—	—
MEAN ^f			-0.51 ± 0.46	4.9 ± 5.8						0.03 ± 0.04

$$\epsilon = -0.5 \exp\left(-\frac{d^2}{2\sigma_b^2}\right), \quad (3)$$

where d is the angular distance of the off-beam centre from the source, and σ_b is the Gaussian width of the beam.

In the case of W-MMD11, our detection level increases from $\simeq 3.0\sigma$ to 3.9σ , after folding in the negative flux density from the outer pixels.

Our sub-mm flux density measurements for all of our targets are presented in Tables 1 and 2, including the upper limits at $450\mu\text{m}$ as well as the $850\mu\text{m}$ data.

2.1.2 Confusion noise

Given that our $850\mu\text{m}$ integrations go relatively faint, we need to be concerned about the issue of confusion noise ([Scheuer 1957; [Scheuer 1974; Condon 1974; Wall et al. 1982]). In other words, we need to consider to what extent the fluctuations due to undetected sources contribute to our error bars. This is additionally complicated by our use of double-difference data, rather than data from fully-sampled maps.

Blain et al. (1998) quote a value of 0.44 mJy for the variance due to confusion, derived from their source counts. We find that any reasonable fit to the counts, including extrapolation to low fluxes (with the constraint of not over-producing the far-IR background) lead to a variance of no more than $\sigma_{\text{conf}} \simeq 0.5\text{ mJy}$. This then is the confusion noise for a single bolometer observation of the sub-mm sky. Since the JCMT gives a triple-beam response, i.e. $\text{On} - (\text{Off}_1 + \text{Off}_2)/2$, then the rms in our photometry observations is expected to be $\sqrt{3/2}$ higher than this, for the simplest configuration. But, since we chopped in azimuth while the sky rotated, then in practice we are taking the central value minus the average of several other sky positions. So the rms of our photometry observations ends up being only a little higher than for an individual bolometer measurement. We checked with Monte Carlo simulations (of sources drawn randomly from reasonable count models) that the confusion noise for our observations was unlikely to be higher than 0.55 mJy . This represents the expected error on our fluxes due to the presence of undetected sources in the beam. We confirmed this value with Monte Carlo simulations of a large number of sources drawn from a model of the number counts.

This confusion noise is already contained in our error bars, and should not be added to the error budget. Our noise estimates come from the variance among the different flux samples of each target. Therefore our noise estimates will already contain at least part of the confusion noise, since the off-beams were sampling different positions on the sky. Hence the variation in the flux of an object throughout the observation period could have partly been due to confusion noise. We believe that the error bars we quote on the flux for each target is a reasonable estimate of the uncertainty in the flux at that central sky position.

Each of our target measurements had a final estimated uncertainty of about 1 mJy . Since confusion and noise and noise from the atmosphere or the instrument add in quadrature, then the contribution from confusion noise is subdominant – contributing less than 30% to the variance. Note also that when we average our measurements together (in

Section 4.1) we can reach, in principle, below both the individual sky/instrumental noise and the confusion noise in each measurement.

2.2 Optical spectroscopy

Spectra for these objects were obtained using the LRIS instrument on the Keck telescope in the course of following up the U -band dropout candidate objects in the survey fields, to confirm their redshifts. Details of the observations can be found elsewhere (Steidel et al. 1996b; Adelberger et al. 2000). Spectra typically show weak $\text{Ly}\alpha$ emission and several absorption lines from the interstellar medium within these galaxies. None of our targetted objects have remarkable optical spectra, strong emission lines being absent for example. Fig. 2 shows the spectra of two representative objects, including the possible sub-mm detection.

3 COMPARING THE UV WITH THE FAR-IR

In order to compare optical (rest-frame UV) observations to our sub-mm (rest-frame far-IR) data we can calculate a far-IR flux consistent with the UV extinction and compare that to our direct SCUBA measurements. Alternatively, we can calculate the SFR implied by each of the data sets (UV and sub-mm) and compare those. For our one detected source, the second, perhaps less direct comparison may help elucidate the underlying physical processes. We list both sets of estimates in Table 1, and now describe how we arrived at the values given there.

3.1 Estimates of star formation rates from the sub-mm data

To estimate the SFR from the measured sub-mm flux density we follow an approach which has become conventional for dealing with *IRAS* galaxies, for example. In essence this involves estimating the $60\mu\text{m}$ flux, which is approximately linearly related to the SFR.

We first calculate the quantity

$$\mathcal{L}_{\text{rest}} \equiv (\nu L_\nu)_{\text{rest}} = 4\pi D_L^2 \nu_{\text{obs}} S_{\text{obs}}, \quad (4)$$

where L_ν is the luminosity density and D_L is the usual luminosity distance. In the rest frame we are observing the galaxy at $850/(1+z)\mu\text{m}$. We then assume that the dust can be described by a mass absorption coefficient of the form

$$k_d = 0.14 (\lambda/850\mu\text{m})^{-\beta_d} \text{ m}^2 \text{ kg}^{-1} \quad (5)$$

(see Hughes et al. 1997 and references therein), with a typical value of $\beta_d = 1.5$ for the index. Note that other authors (e.g. Lisensfeld, Isaak & Hills 2000 and references therein) suggest values of k_d which are smaller by a factor ~ 1.5 ; our dust masses (and other derived quantities) are thus fairly conservative.

Since

$$L_\nu \propto S_\nu \propto k_{d,\nu} B_\nu, \quad (6)$$

with $B_\nu(T_d)$ the Planck function, then we can obtain $\mathcal{L}(60\mu\text{m})$ from $\mathcal{L}(\text{rest})$ using the ratio of $\nu k_{d,\nu} B_\nu$ at the two wavelengths. We also assume for definiteness that $H_0 = 50 \text{ km s}^{-1} \text{ Mpc}^{-1}$ and $\Omega_0 = 1.0$. Both L_{FIR} and SFR (as

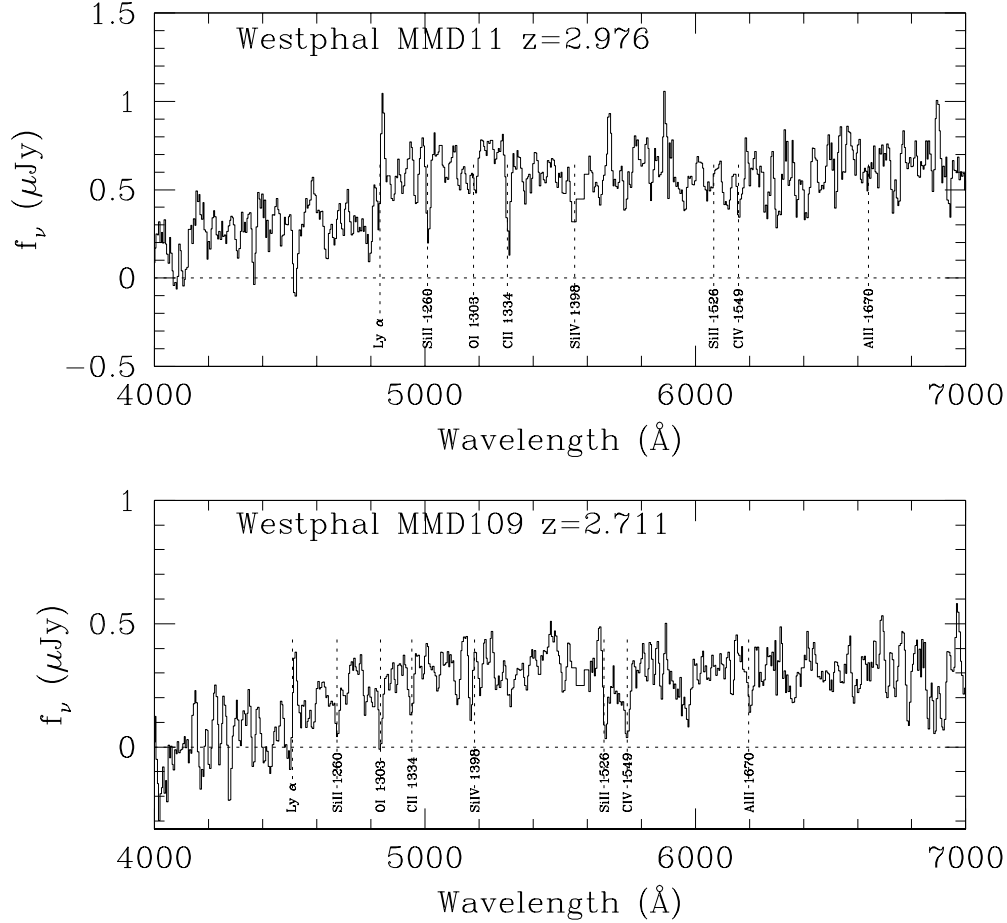


Figure 2. Optical spectra for two representative Lyman break galaxies, obtained using LRIS on Keck. The redshifted wavelengths of Ly α emission and some prominent interstellar absorption lines are marked. Note that the vertical axis depicts only relative flux.

well as inferred properties such as dust mass) scale as h^{-2} , and at these redshifts, the values are about 2 times higher in an open $\Omega_0 = 0.3$ universe.

As an intermediate step we could also estimate the dust mass at this point, assuming that the dust is optically thin. The dust mass estimate is just

$$M_d = \frac{S_{\text{obs}} D_L^2}{k_d^{\text{rest}} B(\nu^{\text{rest}}, T_d) (1+z)} \quad (7)$$

(Hughes et al. 1997), with $B(\nu^{\text{rest}}, T_d)$ the Planck function evaluated in the rest frame, assuming the dust to have a temperature T_d . We take $T_d = 50$ K as our standard value. Note that we are assuming that the full sub-mm flux is due to thermal dust emission. A strong synchrotron flux would

cause our mass estimates to be high. Furthermore if the dust is not entirely optically thin this would also affect the estimate of M_d and correspondingly \mathcal{L} .

We can proceed from the estimate of $\mathcal{L}(60 \mu\text{m})$ to the SFR by firstly applying a bolometric correction, and then using a standard conversion factor. Rowan-Robinson et al. (1997) suggest that $L_{\text{FIR}} \simeq 1.7 \mathcal{L}(60 \mu\text{m})$, where L_{FIR} means the total luminosity over say $1 \mu\text{m}$ – $1000 \mu\text{m}$. The far-IR luminosity is expected to be directly proportional to the star formation rate SFR, i.e.

$$L_{\text{FIR}} = K \times \text{SFR}, \quad (8)$$

where the coefficient K is estimated from well-studied local objects to be $K = 2.2 \times 10^9 L_\odot M_\odot^{-1} \text{ yr}$ (Rowan-Robinson et

al. 1997). Estimates in the literature range from 1.5×10^9 to $4.2 \times 10^9 L_{\odot} M_{\odot}^{-1} \text{ yr}$ (Thronson & Telesco 1986; Scoville & Young 1983). Significant differences between local and distant galaxies could of course change this scaling factor.

Note the limitations of this procedure in assuming an isothermal distribution; dust components with higher temperature, or AGN contributions to the flux, could lead to higher L_{FIR} for the same M_d . The estimated far-IR flux and SFR will also strongly depend on the assumed form of the grey body. Bolometric corrections will typically vary as $T_d^{4+\beta_d}$ (see e.g. Blain et al. 1999c) and so different dust temperatures or emissivity indices can give significantly different results.

We make an empirical estimate of the total uncertainty involved in the dust models by fitting Eq. (6), for $T_d = 50 \text{ K}$, to the long wavelength data for several vigorous star-forming galaxies for which we have rest frame IR data. The discrepancy between our fits at $60 \mu\text{m}$ and the actual data at $\lambda = 850 \mu\text{m}/(1+z) \sim 200 \mu\text{m}$ spans a factor of 3. We adopt this as the uncertainty in L_{FIR} inferred from our SCUBA data (see Hughes & Dunlop 1998 for a recent discussion of the various uncertainties in such estimates).

Fig. 3 provides an illustration of the uncertainties involved in estimating L_{FIR} from measurements at a single wavelength. Dashed curves in Fig. 3 are for model dust emission spectra with $T_d = 30, 50$, and 70 K , normalized to our measurement. Notice that these three curves differ by a factor of three at $\lambda = 60 \mu\text{m}$, the wavelength at which one ordinarily infers the SFR for nearby galaxies. In principle we could use our own $450 \mu\text{m}$ data to remove the uncertainty in dust parameters, but none of our data are precise enough to be very useful. For W-MMD11 we can infer that $T_d \lesssim 90 \text{ K}$, with much weaker limits for the other objects.

The data for our one detected source, W-MMD11, and for our highest sensitivity non-detection, W-DD20, are shown in Fig. 3, along with the redshifted spectrum of a representative star-forming galaxy, M82 (using the model fit from Efstathiou, Rowan-Robinson & Siebenmorgen 1999). W-MMD11 is fairly well approximated by the M82 SED, except for the larger K -band flux. W-DD20, on the other hand, has a much lower sub-mm flux than M82, when normalized to the K and R_s magnitudes; DD20 is clearly not an analogue of nearby starburst galaxies.

3.2 Estimate of the sub-mm flux density directly from the UV

To estimate the $850 \mu\text{m}$ flux, $S_{850-\text{UV}}$ we use the Meurer et al. (1999) empirical relationship between UV slope β and the ratio $L_{\text{FIR}}/\mathcal{L}(1600 \text{ \AA})$, where $\mathcal{L}(1600 \text{ \AA})$ is νL_{ν} at 1600 \AA and L_{FIR} the approximately bolometric dust luminosity as estimated from *IRAS* 60 and $100 \mu\text{m}$ fluxes. From this we can directly estimate the flux at $850 \mu\text{m}$, assuming an isothermal modified blackbody with a dust temperature of 50 K and an emissivity index of 1.5 (see for example Rowan-Robinson et al. 1990). This approach is consistent with the Calzetti law applied to observations of local starburst galaxies (Meurer et al. 1997; Calzetti et al. 1996). Ouchi et al. (1999) have also demonstrated that such a procedure is consistent with the empirical relation for $L_{\text{FIR}}/L_{\text{UV}}$ discussed by Meurer et al. (1997, 1999). Our UV-based predictions for sub-mm emission are listed in Table 1. Note, that the value of K

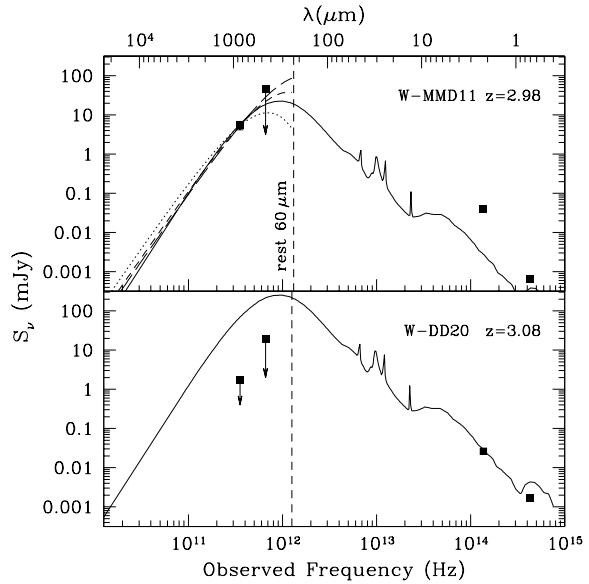


Figure 3. The measured S_{850} , S_{450} , K -band and R_s -band points and 2σ upper limits are plotted for our detection (W-MMD11, upper panel) and also for our target LBG with the highest achieved sensitivity (W-DD20, lower panel). The solid line spectrum shown here is a redshifted version of a nearby star-forming galaxy, M82, adapted from Efstathiou et al. (1999), and normalized to the $850 \mu\text{m}$ point (upper panel) and the near-IR data (lower panel). In the case of W-DD20, the normalization to the optical data points emphasizes the poor fit of this local starburst to the majority of our LBG sample. The dashed lines in the upper panel are grey-body spectra for emissivity $\beta_d = 1.5$ and $T_d = 30, 50$ and 70 K . For nearby galaxies, the *IRAS* $60 \mu\text{m}$ and $100 \mu\text{m}$ bands have typically been used to estimate SFRs (e.g. Meurer et al. 1997). We have marked the location of the $60 \mu\text{m}$ band, in the rest-frame, with a vertical dotted line for both objects, as an indication of the extrapolation used in this study relative to nearby objects. The spread of values of the dust curves at $60 \mu\text{m}$ indicates the level of uncertainties in our dust model.

(from equation (8)) that we use is approximately a factor of 3 *lower* than the effective value used by Meurer et al. (1999). Our results are therefore conservative in the sense that other reasonable estimates could predict even higher sub-mm fluxes, and hence make our non-detections even harder to understand.

3.3 Estimates of star formation rates from the UV spectra

It is worth describing the UV-based SFR estimates in more detail, to reveal various sources of potential uncertainty. The star formation rate is estimated from the rest-frame UV by calculating an implied bolometric luminosity (L_{bol}) and extrapolating to the SFR using an assumed initial mass function (IMF). Dust opacity leads to both a global dimming and a reddening of a galaxy's SED, with the UV region being most affected. We also need to take into account inter-galactic dimming, due to intervening $\text{Ly}\alpha$ blanketing and photoelectric absorption (Madau et al. 1996).

The largest uncertainty in the SFR calculation from the rest frame UV results from the dust extinction. Extinction curves show some environmental dependence, e.g. differences between the Milky Way, the LMC, the SMC and M31 (see Calzetti 1997 for a discussion). With extended objects the effective obscuration is a function of the dust distribution and geometry (Calzetti et al. 1996). We have focussed on the dust effects modelled by Calzetti (1997), which will be referred to hereafter as the Calzetti attenuation law (see also Calzetti et al. 1995, 1996; Calzetti & Heckman 1999; Meurer, Heckman & Calzetti 1999). Meurer et al. (1999) found that their general procedure produced results which were in good agreement with radio data (Richards 2000).

The correction factors used to obtain the UV-corrected SFRs in Tables 1 and 2 are based on the Calzetti attenuation curve. The slope of the UV continuum, usually referred to as β , can be estimated for $z \sim 3$ objects from broad band colours covering the G - and R_s -bands (Steidel et al. 1996a). An unreddened UV stellar continuum slope of $\beta_0 = -2.1$, thought to be appropriate for high redshift stellar populations (Calzetti et al. 1995), is used throughout; the difference between 2.1 and the measured slope indicates the total dust column density. The mean dust correction for the entire LBG sample is ~ 4.5 . The extinction corrections are computed using a 10^9 yr starburst, which is likely to be a conservative assumption since younger starbursts would give bluer intrinsic UV spectra, implying larger reddening corrections and more dust.

The SFR can vary considerably for differences in the assumed reddening curve. The Calzetti model results in larger corrections, by a factor of ~ 2 , than those derived from the SMC (Bouchet et al. 1985). However, reddening curves derived from resolved stars, such as in the SMC, do not include scattered light along the line-of-sight, as do galactic-derived curves. Meurer et al. (1999) have recently shown that under the assumption of an SMC-type reddening curve, the far-IR/far-UV relation observed in local UV-selected star-forming galaxies would not be reproduced, because of this effect. Our corrections to the SFR are based on the properties of local starburst galaxies (which themselves have a far-IR/far-UV flux relation containing considerable scatter, Meurer et al. 1997). This relationship could of course be different at high redshift.

In summary then, we estimate the quantity $\text{SFR}_{\text{UV-corr}}$ as follows. Meurer et al. (1999) express their empirical $\beta \rightarrow L_{\text{FIR}}/\mathcal{L}_{1600}$ relation also as a $\beta \rightarrow A_{1600}$ relation, where A_{1600} is the estimated extinction in magnitudes at 1600 \AA . The SFRs are calculated using the value at 1600 \AA from this relationship to estimate the dust-corrected 1600 \AA luminosity of the LBGs, and then using another relationship (from Madau, Pozzetti & Dickinson 1998) between \mathcal{L}_{1600} and SFR to estimate the star-formation rates. This is a somewhat different method than was used in estimating SFRs from the SCUBA fluxes. We chose to follow two slightly different procedures since one is more familiar in the optical literature and the other in the far-IR literature. The extent to which they are different should also indicate the level of uncertainty.

3.4 Bias caused by uncertainties in the UV-estimated SFR

There is an obvious concern that in selecting those objects with the highest *implied* SFRs we may have preferentially selected statistical outliers which have the biggest positive excursions from the true SFR, which may be considerably lower. In other words, it is more likely that we have overestimated the dust correction factor than underestimated it, due to a Malmquist-type bias. The number density of LBGs with small correction factors (a factor ~ 4 or so) is much higher than the number density with large corrections. As a result, a galaxy which appears to require a large correction factor may actually be an object with a small correction factor and large photometric errors. We have estimated the size of this effect through Monte Carlo estimates of error bars on UV-derived values. In detail, we estimate the intrinsic distributions of dust-obscured luminosities and dust extinctions from our full sample. We can then draw mock LBGs from these distributions, calculating the true colours of the objects, and then measuring their colours using the same procedure as for the real LBGs. From this procedure we can estimate the likely distribution of dust-corrected SFRs for an object with a given redshift and G and R_s magnitudes. This accounts for Malmquist bias, photometric errors and most other potential sources of bias in our selection. The resulting distributions are not symmetric, so we simply calculate the rms scatter in the SFRs for each LBG. These uncertainties in $\text{SFR}_{\text{UV-corr}}$ and $S_{850-\text{UV}}$ are quoted in Tables 1 and 2. The full procedure is described in Adelberger & Steidel (2000).

Further, the uncertainties in the SFR correction factor scale roughly with the magnitude of the correction (Steidel et al. 1998), and there is some danger that the largest implied SFRs are more uncertain than typical. On the other hand, while it is true that the SFR correction factors for our sample are somewhat larger than average for LBGs, in fact the objects with the largest corrected SFRs also have higher than average *uncorrected* SFRs; our targets do not have the steepest UV-slopes of the whole Lyman break sample.

The errors in inferred SFR could conceivably be relatively large compared to the variation in UV parameters – UV luminosity and continuum slope in particular – especially at fainter magnitudes. Monte Carlo simulations (Adelberger & Steidel 2000) reveal that photometric errors of order 0.2 mag in $G - R_s$ affect the corrected SFR by a factor of up to 3.

4 DETECTION OF SOURCES

At $850 \mu\text{m}$, there is one likely detection in our current sample, Westphal-MMD11. We have tried different weightings and edits of the data, and find that the detection is independent of the details of the data analysis. The flux density estimate (the weighted average of all scans, including contribution from off-beams) is about 4σ .

At $450 \mu\text{m}$, we marginally detect Westphal-MM27 at 3σ . The complete absence of flux at $850 \mu\text{m}$ indicates that this is most likely a low redshift foreground object, and we do not consider it further.

No other galaxy among the 16 we observed is detected.

4.1 Statistical results

It is important to ask whether there is statistically a detection of the collective emission from the eight galaxies listed in Table 1. If we combine the $850\,\mu\text{m}$ flux density for all the objects, with inverse variance weighting, the mean is 0.51 ± 0.39 mJy, which is consistent with zero. Omitting W-MMD11, the result is 0.08 ± 0.41 mJy. There is little evidence that, on the average, we obtain positive flux density when we point at our targets. This is to be contrasted with the total signal of 1.46 ± 0.36 mJy predicted from the UV using a dust temperature of 50 K (as shown in Fig. 4), and taking into account simulations of photometric uncertainties. This group of LBGs thus does not form a large part of the population of sub-mm sources. This result points out the power of our approach (see also Scott et al. 2000): statistical analysis of photometry allows us to measure statistical contributions to the source counts, from targetted objects, below 0.5 mJy sensitivity (around the confusion limit for mapping), and for only a modest amount of telescope time.

In order to clarify the constraints for the sample as a whole, in Fig. 4 we plot the actual measured sub-mm flux densities against the predictions for $T_d = 50$ K (solid squares), and also show the predicted lines for 30, 50 and 70 K dust models. A best-fitting slope is consistent with zero, and certainly inconsistent with the measured flux densities being equal to the UV-predicted ones (dashed line labelled ‘50 K’, for which $\chi^2 = 21.6$ for the 7 undetected objects, using the vertical error bars).

Another statistical approach to the data set is to ask how much lower the SFR has to be compared with the UV-based estimates. We constrain the factor f in the relation $\text{SFR}_{\text{submm}} = f \text{SFR}_{\text{UV-corr}}$, by minimizing the variance for the entire sample. We find that $f = 0.04 \pm 0.24^*$ if we exclude the detected object, and the straight line is a reasonable fit. However, if we include the detection we obtain a high value for f but a terrible χ^2 , indicating that W-MMD11 is very much an outlier compared with the other seven galaxies. Excluding W-MMD11 then, the corresponding 95 per cent upper limit is $f < 0.50$, indicating that for our undetected objects, the sub-mm flux densities are overestimated by a factor of at least 2. This could be due to either a higher temperature, or one of the other factors assumed in converting from UV to sub-mm properties. Many of these uncertainties are dealt with in our Monte Carlo studies, as indicated by the rms errors in Table 1. If these (horizontal) error bars are included in the fit, then $f = 1$ cannot be very strongly excluded.

Focussing specifically on dust temperature, if we assume that all the other parameters are held fixed, the seven galaxies (aside from W-MMD11) in Table 1 are best described by very hot dust, at or even above 100 K. The 95 per cent confidence lower limit for T_d is 65 K.

4.2 Lyman break galaxies in the HDF

The HDF has been mapped deeply with SCUBA (Hughes et al. 1998). There are two LBGs from our catalogue lying

* This is using only the observational (vertical) error bars. If we were to take into account the estimated horizontal error bars, we would obtain $f = 0.07 \pm 0.39$.

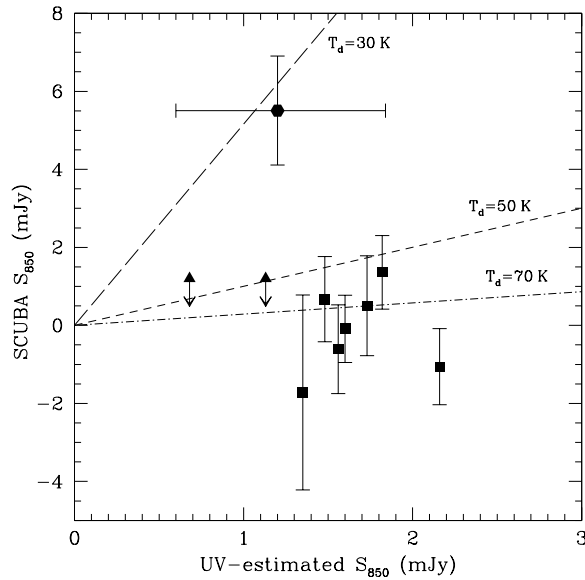


Figure 4. Measured SCUBA $850\,\mu\text{m}$ flux densities, with 1σ error bars, plotted against $850\,\mu\text{m}$ flux density predicted from the UV properties and simple assumptions about star formation for $T_d = 50$ K. Horizontal error bars are shown on our one detection only, but should be indicative of the errors for the rest of the points. Although in practice the distributions are quite skewed, we have shown the rms as a symmetric error bar for simplicity. These errors reflect uncertainties in photometry and other biases as estimated using Monte Carlo simulations. Our detection (W-MMD11) is plotted as a solid hexagon with 1σ error bars. We also show 2σ upper limits for the 2 high SFR UV-corr LBGs lying in the Hubble Deep Field (triangles). The dashed lines show the locus around which the points would scatter if the UV deficit is re-radiated at $T_d = 30, 50$, and 70 K. A best-fitting straight line to the data is consistent with zero, indicating that the UV-predicted flux densities are on average too high by at least a factor of ~ 2 , as discussed in the text.

within the Hubble Deep Field which also have a high UV-implied SFR ($\sim 150 M_\odot \text{yr}^{-1}$), corrected using the Calzetti attenuation curve. None of the 5 sources detected in the deep HDF SCUBA map correspond with the positions of these two LBGs. When combined with our results (Table 1), this increases to 9 the number of high SFR LBGs which are undetected at a 3σ level of ~ 4 mJy. What we see for the HDF upper limits (Fig. 4) is that the UV-based predictions of the far-IR flux density continue to overestimate that measured by SCUBA (even for objects with somewhat less extreme intrinsic luminosities than those in our sample). Thus the HDF non-detections support our conjecture that the simplest UV-predicted sub-mm flux densities are off by at least a factor ~ 2 .

4.3 Westphal MMD11

The first question to address is whether it is very improbable to have found one or more $\sim 4\sigma$ detections purely by chance, given that we searched a relatively large number of objects. The simplest statistical estimate is that, for our full sample

of 16 targets, there is roughly a 5 per cent chance to obtain a spurious 4σ detection by statistical fluctuation alone (2.5 per cent for our revised sample of 8 presented in Table 1).

Next we should assess the possible contamination by the sorts of galaxies which turn up in blank field observations with SCUBA. The probability that a random galaxy lies within the beam is given by $P = 1 - \exp(-\pi n \theta^2)$, where $n(> S)$ is the cumulative surface density for the population in question, and θ is the beam radius. For a flux density of 5.5 mJy the source counts are about 1000 per square degree (e.g. Blain et al. 1999b), and so $P \simeq 1$ per cent per pointing. The chance that at least one of our 16 observations yields a 5.5 mJy source is then ~ 15 per cent (or about half of that if only our revised sample of 8 likely sub-mm candidates is considered). It is then statistically conceivable that the positive flux density for W-MMD11 could be completely unassociated with the LBG, and instead due to a random sub-mm-bright galaxy within the same SCUBA beam. As we argue below, circumstantial evidence for the LBG suggests that it is indeed the source of the sub-mm emission. But without high resolution sub-mm observations of this region we cannot discount the interloper possibility entirely.

There is, in fact a foreground galaxy which has slightly corrupted the UV measurements of W-MMD11. Fig. 2 (top panel) presents a Keck spectrum of W-MMD11, with some of the usual lines identified. Because of a brighter object partially on the same slit, the continuum of W-MMD11 is over-subtracted. The resulting spectrum then has a slope which is inconsistent with the very red $R_s - K$ colour. For comparison the bottom panel of Fig. 2 shows the optical spectrum for another of our targetted LBGs, W-MMD109, which is typical of the remainder of the galaxies in the sample (note that the vertical axis on the figure depicts only relative flux). The spectrum of W-MMD11 is similar except for contamination by the foreground object (4.0 arcsec North and 0.5 arcsec East of W-MMD11), with little indication of strong emission lines for example.

W-MMD11 is, however, bright in K -band ($K \sim 19.6$), and with $R_s - K = 4.45$, which is about 1.5 mag redder than average for those LBGs for which near-IR photometry has been obtained. In fact, out of 70 LBGs for which we currently have K -band photometry, only one is redder than W-MMD11. Following recent discoveries that at least some $z > 2$ SCUBA sources can be identified with galaxies having extremely red near-IR colours (Smail et al. 1999a), this argues in favour of the identification of the SCUBA detection with the LBG, W-MMD11.

We discount the possibility that the particular foreground object is actually the sub-mm source. This nearby source is at $z = 0.532$, with the [O II] line having a rest equivalent width of 49 Å, which is somewhat on the high side for general field galaxies. However, it has magnitudes $R_s = 22.16$, $G - R_s = 0.88$ and $U_n - G = 0.54$, indicating a normal, somewhat sub- L^* galaxy, which would not be expected to emit strongly at sub-mm wavelengths. We estimate that it could contribute at most 0.6 mJy to the integrated flux density within the SCUBA beam centred on W-MMD11, based on nearby spiral galaxies (Krugel et al. 1998).

The most likely explanation for the positive flux density is that we have detected the LBG, which is re-enforced by

the red $R - K$ of this LBG relative to the others in our sample. We treat it as a detection in the discussion below.

4.4 Comparing LBGs to sub-mm selected galaxies

The LBG which is detected with SCUBA, W-MMD11, has a large $R_s - K$ colour in addition to its extreme rest-frame UV properties. Moreover, only about 10 per cent of the whole current sample of LBGs (> 700 objects) are redder than W-MMD11 in terms of $G - R_s$ colour, and only 10 per cent are brighter in R_s magnitude. It is worth exploring how these features compare with other known high redshift SCUBA sources.

We have obtained or derived filter-matched data in the R_s , G and U_n filter set (Steidel et al. 1998) for the two high- z sub-mm selected galaxies with secure redshifts: SMM J02399–0136 (Ivison et al. 1998b) and SMM J14011+0252 (Ivison et al. 1999b), with the aim of understanding whether our selection techniques successfully predict the measured sub-mm flux densities (explicitly, we made filter corrections for the first object, and reobserved the second object). Table 3 directly compares these three sub-mm bright galaxies. The conclusion is that SMM J02399–0136 and SMM J14011+0252 are very similar to W-MMD11, although possibly more luminous (the lensing amplification by a foreground cluster may be uncertain by up to 50 per cent). We also note that SMM J02399–0136 is thought to have an AGN component (Ivison et al. 1998b), and thus would probably have been excluded from our sample of LBGs to be studied with SCUBA.

Other LBGs with large UV-derived star-formation rates ($> 100 M_\odot \text{ yr}^{-1}$), but rather modest $R - K$ colours, were not detected with SCUBA at the ~ 0.5 mJy rms level (when averaged together). This implies that K -band information may help significantly to pre-select sub-mm bright LBGs. However, photometric errors conspire to make it difficult to know whether any particular UV-selected object is truly a prodigious star former, at the level of the SCUBA-selected sources.

For the two SCUBA-selected objects in Table 3, the sub-mm flux densities and ratio, (S_{450}/S_{850}) , are consistent with what we would predict from the UV magnitudes and slope (see section 3.3) using a dust temperature of ~ 50 K and emissivity $\beta_d = 1.5$. SMM 02399 is better modelled by a lower dust temperature ($T_d \simeq 40$ K) while SMM 14011 is better modelled by a higher dust temperature ($T_d \simeq 60$ K). This implies that the technique of predicting the dust emission from the UV parameters is reasonably sound if the dust temperature distribution is known. However, the 850 μm flux density for W-MMD11 is under-predicted, unless the dust temperature used is much lower (say $T_d = 32$ K). This is in strong contrast to the results for the rest of the LBGs which would indicate quite a hot T_d if we fixed all the conversion factors at typical values. Of course, different temperatures are not the only explanations for why we detect W-MMD11 alone. Another possibility is that the spatial distribution of the dust could have given rise to a detection in emission, but less effect on the absorption properties.

Although our targetted sample are not particularly bright in the sub-mm, recent simulations (Adelberger & Steidel 2000) suggest that *some* of the LBGs in the total sample must have large enough SFRs to be detected

Table 3. Comparison of the LBG detection W-MMD11, with two high- z SCUBA-selected objects with confirmed redshifts, SMM J02399–0136 and SMM J14011+0252.

Property	W-MMD11	SMM J02399–0136 ^{a,b}	SMM J14011+0252 ^c
z	2.979	2.803	2.550
$U_n - G$	2.04	2.19	1.65
$G - R_s$	1.04	1.00	0.69
$R_s - K$	4.59	3.70	3.54
S_{850} (mJy)	5.5 ± 1.4	10.4 ± 1.2	5.3 ± 0.7
S_{450} (mJy)	22.0 ± 23.4	27.6 ± 6.0	15.2 ± 2.5
UV-predicted flux densities			
S_{850-UV}^d (mJy)	1.2 (3.1)	4.3 (11.1)	8.0 (21.1)
S_{450-UV}^d (mJy)	4.1 (10.6)	13.2 (34.3)	27.4 (51.0)

^a Ivison et al. 1998a – lensing factor of 2.50 assumed.

^b Note that this object has the spectrum of an AGN in the UV and so may not conform to the far-IR/UV relation.

^c Ivison et al. 1999b – lensing factor of 2.75 assumed.

^d Predicted from UV colours, assuming a dust temperature of 50 K (or 38 K in brackets – corresponding to Blain et al. 1999b).

with SCUBA ($> 400 M_\odot \text{ yr}^{-1}$). The most likely galaxies to be detected might be those with brighter apparent magnitudes and smaller implied dust corrections, since errors in R_s are smaller than errors in $G - R_s$, and the corrected star-formation rates are less sensitive to errors in R_s than in $G - R_s$. Although some galaxies in our sample are already of this type (our detection W-MMD11 being one of them), this possibility should be further checked in future with separate samples. Also, as deep K -band photometry becomes available for the LBG samples, the $R - K$ colour may prove to be a useful selection criterion for sub-mm follow-up. Indeed, several SCUBA-selected galaxies, beyond those with known redshifts discussed in section 4.3, are now believed to have optical counterparts with very red $R - K$ colours (Smail et al. 1999a) classifying them as Extremely Red Objects (see for example Dey et al. 1998).

5 DISCUSSION

There is currently a great deal of debate on reconciling the various techniques for estimating the SFR using different wavelength regimes, such as sub-mm, UV continuum or $H\alpha$ (see for example: Kennicutt 1998; Ouchi et al. 1999; Cowie, Songaila & Barger 1999). Regardless of the precise relationships between SFR estimators, we can certainly say that the LBGs with the largest expected SFRs are apparently not excessively bright sub-mm emitters, and are less luminous than the typical sub-mm sources discovered in a SCUBA ‘blank field’ survey (Smail et al. 1997; Barger et al. 1998; Hughes et al. 1998; Lilly et al. 1999).

As discussed in section 4.2, if we assume that the SCUBA flux density is proportional to the UV-predicted flux density, then our data can be used to infer that the UV-predicted flux densities are on average too high by factors of a few, depending on the dust temperature. For $T_d \lesssim 50$ K this factor would be even higher, while for $T_d \gtrsim 70$ K, the UV predictions are consistent with the measured SCUBA flux densities, within uncertainties. By contrast, the detection (W-MMD11) in our sample is at a level *above* that im-

plied by the UV calculations, even for unusually cool dust temperatures.

Since we currently have only a small sample of sufficiently deep integrations, including one probable detection, we cannot conclude from our results that *all* LBGs are likely to be weak sub-mm emitters. As discussed in section 3.3, recent results (Adelberger & Steidel 2000) suggest that the LBGs with the largest SFR correction factors (e.g. W-MMD109 in Table 1) are probably subject to larger UV photometric and Malmquist-type errors, and have lower corrected SFRs when the uncertainties are taken into account. This could lead to a situation where only a few of the galaxies in this sample truly have large SFRs, which would also be consistent with our observations.

On the other hand, we should emphasize that there is no reason a priori to assume that the high redshift galaxies have a similar relationship between far-IR/far-UV flux and UV continuum slope to the local starburst population, which itself has large scatter (Meurer et al. 1999). This may well play a role in any discrepancy between our sub-mm data and predictions based on the UV. A reasonable conclusion is therefore that the simplest predictions for SCUBA flux densities for our targets are on the average overestimated by a factor of order a few. The precise reason for this is difficult, at present, to ascertain.

5.1 Relationship with sub-mm selected sources

The central question remains: is there any overlap between samples selected as LBGs and SCUBA-detected blank field sources, when they are at the same redshift? The difficulty in obtaining accurate optical counterparts and redshifts for the sub-mm sources means that the volume and luminosity function of sub-mm ‘blank field’ surveys is still essentially unknown. Initial spectroscopic follow-up (Barger et al. 1999; Lilly et al. 1999) has suggested that a significant fraction of the SCUBA population does not lie at $z > 2$. However, use of the Carilli and Yun (1999) relation of radio/far-IR flux to predict the redshifts for a large sample of SCUBA sources (Smail et al. 1999b), has suggested that the population may

have a median value lying between $z=2.5-3$. It is worth noting that the detection of W-MMD11 in our sample currently represents the highest redshift source detected with SCUBA, which is not an AGN.

This one detection suggests that with reasonable SCUBA integrations we might expect to detect just those few LBGs that are far-IR brightest. This would be consistent with ‘blank field’ sources lying over a wider range of redshifts than that probed by the U -band drop-out selection technique, where a few extreme specimens at any given epoch radiate strongly in the sub-mm. The fact that our high SFR Lyman break sample is on average undetected in the sub-mm implies that probably only the very highest star formers would constitute part of the blank-field sub-mm sources. LBGs might also be harder to detect if they had higher dust temperatures (as depicted in Fig. 4).

We now consider scenarios which are consistent with our data and in which the population of LBGs is indeed related to the population of sub-mm selected sources. If none of these proves plausible one could always consider the possibility that the relationship between far-IR and far-UV flux, and UV continuum slope to be different at high redshift than it is for local starburst galaxies.

If many of the blank field sub-mm sources are in fact star-forming, merging galaxies at even higher redshifts ($z \sim 4-5$), as yet undiscovered in optical surveys, they might represent an era when the star formation was much more vigorous and short lived. Recent results (Steidel et al. 1998) have revealed more $z \sim 4$ LBGs than implied by number counts and modelling of data from the HDF. These are not expected to be strong sub-mm emitters, since a similar colour range to the $z \sim 3$ population is observed. Massive merging fragments are now thought to be responsible for the prodigious SFRs observed in many SCUBA sources (Blain et al. 1999a), perhaps implying more SCUBA-bright sources during the period of most merging activity. But certainly, accurate prediction of sub-mm properties from optical properties will await a more complete understanding of the galaxy formation process.

Recent observations have revealed possible analogues to the ‘blank field’ discovered sub-mm sources (Ivison et al. 1998b; Chapman et al. 1999), where the sub-mm flux density is likely to be dominated by AGN heated dust. It is possible that spectroscopic follow up of ‘blank field’ sources may reveal that more are AGN dominated, implying a large population of high redshift dusty quasars. Indeed consideration of x-ray results suggest that a significant fraction of the submm sources could involve active galaxies (Almaini, Lawrence & Boyle 1999). If the primary engines powering these sub-mm sources are AGNs, then there may indeed be little relation between these galaxies and the Lyman break population.

Both the LBGs and SCUBA-selected sources are thought to be associated with elliptical galaxies in the process of formation. They can be reconciled if the dust content of young galaxies is coupled to their mass or luminosity, with more massive galaxies being dustier (Dickinson 1998). The most massive young elliptical galaxies could then be associated with the sub-mm sources, while the Lyman break population would be identified with less massive ellipticals and bulges. To verify this possibility, accurate identifications and dynamical mass estimates of the sub-mm galaxies are

required, which may have to wait for the next generation of sub-mm interferometers to detect CO lines (see e.g. Stark et al. 1998).

5.2 Contribution to the far-IR background

One assessment of the significance of the sub-mm emission of LBGs is to estimate their contribution to the IR background at $850 \mu\text{m}$. We can calculate this using the average implied SFRs obtained using the same methods outlined here, together with the surface density estimate for $z \sim 3$ LBGs. We find that typical redshift 3 LBGs then account for about 0.2 per cent of the $850 \mu\text{m}$ background estimates (Fixsen et al. 1998; Lagache et al. 1999). From our SCUBA observations, we find no evidence that the LBG population contributes more than this. However, W-MMD11 is actually much *more* SCUBA-bright than predicted, and so the full contribution will depend on how common such objects are in the LBG population, which we certainly cannot estimate from our small sample.

A significant problem with this estimate is that there is a strong bias, in present samples, against selecting just the sorts of LBG candidates which might dominate the far-IR background. This bias arises from several causes: highly reddened objects have colours satisfying our UGR selection criteria over a much shorter range of redshifts than for bluer objects; at fixed SFR a much smaller fraction of reddened than unreddened objects will satisfy the $R_s < 25.5$ magnitude cut; and red objects tend to be so faint in G that they are difficult to detect and recognize as LBGs down to the R_s limit. We certainly know that highly reddened LBGs are very underrepresented in the current sample, and it is impossible to accurately estimate the $850 \mu\text{m}$ flux for the whole LBG population without fully understanding the relevant selection biases. Because of these biases, it is still possible that the $z \sim 3$ LBG population contributes a significantly higher portion of the background radiation at these wavelengths.

6 CONCLUSIONS

(i) On average we find that the $850 \mu\text{m}$ flux density must be at least 2 times lower than the simplest predictions obtained from the UV colours. This could be accounted for by a combination of photometric errors, uncertainties in T_d , β_d , or the estimates of L_{bol} from the rest-frame UV and far-IR wavelengths or from the scatter in the UV-slope/far-IR relation. Our sample also had some bias against the most highly reddened objects.

(ii) In the case of the detection of W-MMD11, the flux density is a factor ~ 5 times greater than predicted by the UV for dust temperatures $T_d > 50 \text{ K}$.

(iii) The similarities in the properties of W-MMD11 and SCUBA-selected sources of known high redshift, SMM J02399–0136 and SMM J14011+0252, suggest that the large UV-implied SFR in conjunction with a red $R-K$ colour may be a good indicator of significant sub-mm flux density. The comparison may indicate that the prediction of far-IR flux density from UV colours is fairly reliable, even for quite reddened objects, provided that parameters, such as the dust temperature are known reasonably well.

(iv) Estimates for the contribution of the $z \sim 3$ LBGs to the far-IR background give around 0.2 per cent. Our non-detections certainly provide no evidence that the contribution is significantly higher than this. However, given the fact that our one detection has considerably larger sub-mm flux than predicted, and that there are selection biases against highly redenned objects, it is difficult to estimate precisely the overall contribution to the far-IR background.

Our detection of W-MMD11 certainly indicates that there is some overlap between $z \sim 3$ LBG and SCUBA galaxies. However, our small sample makes it hard to draw any firmer conclusions about how great the overlap might be. It also remains to be seen whether the galaxies contributing to the bulk of the far-IR background, over the full range of redshifts, would be also be selected by the UV-dropout technique. Further progress will require significantly more telescope time to improve the sub-mm limits and detections. We have shown that targetted SCUBA photometry is a useful approach here. With larger sub-mm data sets, and selection of LBG samples in different ways, it should be possible to test the predictive power of the far-UV for luminous star forming galaxies at high redshift, and to more fully investigate the role of dust in the galaxy formation process.

ACKNOWLEDGMENTS

This work was supported by the Natural Sciences and Engineering Research Council of Canada. The James Clerk Maxwell Telescope is operated by The Joint Astronomy Centre on behalf of the Particle Physics and Astronomy Research Council of the United Kingdom, the Netherlands Organisation for Scientific Research, and the National Research Council of Canada. We would like to thank the staff at JCMT for facilitating these observations. We are also grateful to Remo Tilanus and his colleagues for their willingness to discuss their own LBG observations.

REFERENCES

- Adelberger K., Steidel C.C., 2000, submitted to ApJ (astro-ph/0001126)
- Almaini O., Lawrence A., Boyle B., MNRAS, 305, L59
- Barger A. J., Cowie L. L., Sanders D. B., Taniguchi Y., 1998, Nat, 394
- Barger A. J., Cowie L. L., Smail I., Ivison R. J., Blain A. W., Kneib J.-P., 1999, AJ, 117, 265
- Blain A. W., Jameson A., Smail I., Longair M. S., Kneib J.-P., Ivison R. J., 1999, MNRAS, 309, 715
- Blain A. W., Kneib J.-P., Ivison R. J., Smail I., 1999, ApJ, 512, L87
- Blain A. W., Smail I., Ivison R. J., Kneib J.-P., 1999d, MNRAS, 302, 632
- Borys C., Chapman S. C., Scott D., 1999, MNRAS, 308, 527
- Bouchet, P., Lequeux, J., Maurice, E., Prevot, L., Prevot-Burnichon M. L., 1985, A&A, 149, 330
- Bruzual A. G., Charlot, S., 1993, ApJ, 405, 538
- Calzetti D., 1997, AJ, 113, 162
- Calzetti D., Heckman T. M., 1999, ApJ, 519, 27
- Calzetti D., Bohlin R. C., Kinney A. L., Storchi-Bergmann T., Heckman T. M., 1995, ApJ, 443, 136
- Calzetti D., Kinney A. L., Storchi-Bergmann T., 1996, ApJ, 458, 132
- Carilli C. L., Yun M. S., 1999, ApJL, 513, L13
- Chapman S. C., Scott D., Lewis, G., Borys C., Fahlman G. G., 1999, A&A, 352, 406
- Chapman S. C., Scott D., Borys C., Fahlman G. G. 2000, in preparation
- Condon, J. J., 1974, ApJ, 188, 279
- Cowie L. L. Songaila A., Barger A. J., 1999, AJ, in press astro-ph/9904345
- Dickinson, M. E., 1998, in M. Livio, S. M. Fall & P. Madau, ed., The Hubble Deep Field, in press (astro-ph/9802064)
- Eales S. A. et al., 1999, ApJ, 515, 518
- Efstathiou A., Rowan-Robinson M., Siebenmorgen R., 2000, MNRAS, 313, 734
- Fixsen D. J. et al., 1998, ApJ, 508, 123
- Groth E. J., Kristian J. A., Lynds R., O'Neil E. J., Balsano R., Rhodes J., and the WFPC-1 IDT, 1994, BAAS, 26, 1403
- Holland W. S. et al., 1998, Nat, 392, 788
- Holland W. S., et al. 1999, MNRAS, 303, 659
- Hughes D. H., Dunlop J. S., Rawlings S., 1997, MNRAS, 289, 766
- Hughes D. H., Dunlop J. S., 1998, in 'Highly Redshifted Radio Lines', eds. C. Carilli et al., PASP Conference Series, in press (astro-ph/9802260)
- Hughes D. H. et al., 1998, Nat, 394, 241
- Ivison R. J., Archibald E. N., Dey A., Graham J. R., 1997, in Wilson A. ed., The Far-Infrared and Submillimetre Universe. ESA publications, Noordwijk, p. 281
- Ivison R. J. et al., 1998a, ApJ, 494, 211
- Ivison R. J., Smail I., Le Borgne J.-F., Blain A. W., Kneib J.-P., Bézécourt J., Kerr T. H., Davies J. K., 1998b, MNRAS, 298, 583
- Ivison R. J., Smail I., Blain A., Kneib J.-P., Frayer D., 1999a, in Proc. 1998 Ringberg workshop on ultraluminous galaxies, in press (astro-ph/9901361)
- Ivison, R. J., Smail, I., Barger, A. J., Kneib, J.-P., Blain, A. W., Owen, F. N., Kerr, T. H., Cowie, L. L., 1999b, MNRAS, submitted.
- Jenness T., Lightfoot, J. F., 1998, in Albrecht, R., Hook, R. N., Bushouse, H. A., eds, ASP Conf. Ser. Vol. 145, Astronomical Data Analysis Systems and Software. Astron. Soc. Pac., San Francisco, p. 216
- Kennicutt R. C., 1993, ApJ, 272, 54
- Krugel, E., Siebenmorgen, R., Zota, V., Chini, R., 1998, A&A, 331, 9
- Lagache G., Abergel A., Boulanger F., Désert F. X., Puget J.-L., 1999, A&A, 344, 322
- Lilly S. J., Le Fèvre O., Hammer F., Crampton D., 1996, ApJ, 460, L1
- Lilly S. J. et al., 1999, ApJ, 518, 641
- Lisenfeld U., Isaak K. G., Hills R., 2000, MNRAS, 312, 433
- Madau P., Ferguson H. C., Dickinson M. E., Giavalisco M., Steidel C. C., Fruchter A., 1996, MNRAS, 283, 1388
- Madau P., Pozzetti L., Dickinson M. E., 1998, ApJ, 498, 106
- Meurer G. R., Heckman T. M., Leitherer C., Kinney A., Robert C., Garnett D. R., 1995, AJ, 110, 2665
- Meurer G. R., Heckman T. M., Leibert M. D., Leitherer C., Lowenthal J., 1997, AJ, 114, 54
- Meurer G. R., Heckman T. M., Calzetti D., 1999, ApJ, 521, 64 (astro-ph/9903054)
- Ouchi M., Yamada T., Kawai H., Ohta K., 1999, ApJ, 517, L190
- Pettini M., Kellogg M., Steidel C. C., Dickinson M., Adelberger K. L., Giavalisco M., 1998a, ApJ, 508, 539
- Richards E. A., 2000, ApJ, 533, 611
- Rowan-Robinson M., Hughes J., Veda K., Walker D. W., 1990, MNRAS, 246, 273
- Rowan-Robinson M., et al., 1997, MNRAS, 289, 490
- Scheuer P. A. G., 1957, Proc. Camb. Phil. Soc., 53, 764
- Scheuer P. A. G., 1974, MNRAS, 166, 329
- Scott D., et al., A&A, in press (astro-ph/9910428)

- Scoville N. Z., Young J. S., 1983, ApJ, 265, 148
 Smail I., Ivison R. J., Blain A. W., 1997, ApJ, 490, L5
 Smail I., Ivison R. J., Blain A. W., Kneib J.-P., 1998a, ApJ, 507, L21
 Smail I., et al., 2000a, MNRAS in press (astro-ph/9905246)
 Smail I., Ivison R. J., Owen F. N., Blain A. W., Kneib J.-P., 2000b, ApJ, 528, 612
 Stark A. A., et al., 1998, in Phillips T. G. ed., Advanced Technology MMW, Radio and Terahertz telescopes. Proc. SPIE vol. 3357, SPIE, Bellingham, in press (astro-ph/9802326)
 Steidel C. C., Hamilton D., 1993, AJ, 105, 2017
 Steidel C. C., Adelberger K. L., Dickinson M., Giavalisco M., Pettini M., 1998, in Proc. Xth Rencontres de Blois, The Birth of Galaxies
 Steidel C. C., Giavalisco M., Dickinson M., Adelberger K. L., 1996a, AJ, 112, 352
 Steidel C. C., Giavalisco M., Pettini M., Dickinson M., Adelberger K. L., 1996b, ApJ, 462, L17
 Steidel C. C., Pettini M., Hamilton D. 1995, AJ, 110, 2519
 Thronson H., Telesco C., 1986, ApJ, 311, 98
 Tresse L., Maddox S. J., 1998, ApJ, 495, 691
 Wall J. V., Scheuer P. A. G., Pauliny-Toth I. I. K., Witzel A., 1982, MNRAS, 198, 221
 Williams R. E., et al., 1996, AJ, 112, 1335